J Mater Sci (2011) 46:548–557
DOI 10.1007/s10853-010-5016-0

Alkaline hydrothermal kinetics in titanate nanostructure formation

Dana L. Morgan · Gerry Triani · Mark G. Blackford · N. A. Raftery · Ray L. Frost · Eric R. Waclawik

Received: 1 August 2010 / Accepted: 19 October 2010 / Published online: 30 October 2010

Abstract In this study, the mechanism of precursor dissolution and the influence of kinetics of dissolution on titanate nanotube formation were investigated. This comparative study explored the dissolution kinetics for the case of commercial titania powders, one composed of predominantly anatase (>95%) and the other rutile phase (>93%). These nanoparticle precursors were hydrothermally reacted in 9 mol L^{-1} NaOH at 160 °C over a range of reaction times of between 2 and 32 h. The high surface area nanotube-form product was confirmed using X-ray diffraction, FT-Raman spectroscopy, and transmission electron microscopy. The concentration of nanotubes produced from the different precursors was established using Rietveld analysis with internal and external corundum standardization to calibrate the absolute concentrations of the samples. Interpretation of the dissolution process of the precursor materials indicated that the dissolution of anatase proceeds via a zero-order kinetic process, whereas rutile dissolution is through a second-order process. The TiO_2 nanostructure formation process and mechanism of TiO_2 precursor dissolution was confirmed by non-invasive dynamic light scattering measurements. Significant observations are that nanotube formation occurred over a broad range of hydrothermal treatment conditions and was strongly influenced by the order of precursor dissolution.

D. L. Morgan · R. L. Frost · E. R. Waclawik (✉)
Chemistry Discipline, Faculty of Science and Technology, Queensland University of Technology, GPO Box 2434, Brisbane, QLD 4001, Australia
e-mail: e.waclawik@qut.edu.au

G. Triani · M. G. Blackford
Institute of Materials Engineering, PMB 1, Australian Nuclear Science and Technology Organisation, Menai, NSW 2234, Australia

N. A. Raftery
X-ray Analysis Facility, Queensland University of Technology, GPO Box 2434, Brisbane, QLD 4001, Australia

Introduction

Advanced understanding of the reaction conditions that determine phase formation is crucial for the successful technological application of chemically synthesized nanomaterials [1]. The wide bandgap semiconductor titanium dioxide (TiO_2) is of particular interest in this regard since it has potential uses in a wide variety of catalytic and photocatalytic processes [2, 3]. In the case of photocatalysis by nanostructured titania films, the performance is largely dependent on the nanomaterial's surface-to-volume ratio which critically depends on the morphology as well as phase and particle size. The morphology can be affected not only by the primary nanoparticle dimensions of an as-synthesized material but also by the secondary particle distribution; hence, it is important to control the particle size and agglomerate distribution both during synthesis and film deposition [4]. Titania nanostructures have been prepared in a number of ways—by sol–gel synthesis, template synthesis, and atomic layer deposition (ALD) for instance [5], but by far the simplest and most cost effective one-pot preparation route is hydrothermal synthesis. Alkaline hydrothermal treatment pioneered by Kasuga et al. [6, 7] in 1998 has been widely examined for the synthesis of titanate nanotubes, nanoribbons, nanofibers, and nanorods. This synthesis regime involves the treatment of a TiO_2 precursor with an alkaline solution (commonly sodium hydroxide) at elevated temperature. An advantage of this hydrothermal method is that the average nanomaterial morphology and dimensions can be controlled by adjusting the processing

time, alkaline concentration, and temperature [8–10]. For example, when the temperature is elevated above 160 °C nanoribbons form in preference to nanotubes [11]. There are numerous potential applications for nanotubes synthesized through alkaline hydrothermal treatment, which include but are not limited to sorbents [12, 13], catalysts [14, 15], and storage devices [16, 17].

Nanotubes are commonly believed to form through the dissolution and subsequent recrystallization of the particulate precursor into single- or multiwalled nanosheets [18, 19], which then scroll or wrap into nanotubes, driven by the saturation of undercoordinated sites or "dangling bonds" [18, 20]. Although many studies have examined the formation of titanate nanotubes, few have examined the effect that dissolution of the TiO_2 crystallites have on the nanotube formation [19]. The dependency of TiO_2 crystallite size is significant, partly because commercial uptake of nanotube-only materials in catalysis and other applications will ultimately rely on the few commercial sources of TiO_2 precursor feedstocks available in large quantities. The efficacy of hydrothermal production of nanotube forms of titania will ultimately be determined by the precursor supply, phase type and form.

Dissolution is a complex process which is often observed in nature through geological processes such as the formation of soils through the weathering of minerals [21], and through the partial melting of mantle and crustal rocks forming magmas [22]. Although the mechanism of dissolution is imperfectly understood, it is generally believed to involve three component processes: (i) interface reaction, (ii) diffusion, and (iii) complications due to convection [22]. At the solid–liquid interface, the surface of the solid is covered with adventitious dissolved species from the bulk solution adsorbed onto the solid's surface. These adsorbed species alter the surface chemistry and reactivity of the solid. The reactivity of this surface determines the intrinsic maximum rate of dissolution. The process of diffusion, which involves the mass transport of reactants from the bulk of the solution to the surface and of products from the surface into solution determines whether or not this maximum rate may be attained [22]. Convection currents affect the diffusion and interface reaction rates making it more difficult to determine the rate-limiting process occurring within the system. Dissolution processes are also governed by the reactants involved and may proceed through ligand-assisted, proton-promoted or reductive processes [21]. The number and type of active surface sites also affects the rate of dissolution, with surface defects including kinks, steps, dislocations, pits, and adatoms generally providing surface sites of lower activation energy and faster rates of reaction than non-defected surfaces [21, 23].

Although TiO_2 is a sparingly soluble mineral with slow dissolution kinetics, the solubility of both anatase and rutile has been observed to increase with elevated temperature and for various pH conditions [24–26]. This implies that nanotubes can be formed through the dissolution of either TiO_2 phase, irrespective of original preconceptions regarding rutile [27, 28]. Within the literature, nanotubes have been successfully produced through the alkaline treatment of anatase, rutile, and brookite [8, 10, 29]. Anatase has often been observed to react rapidly and completely when hydrothermally treated under sufficient conditions (temperature, alkaline concentration, duration) [8, 9, 11, 19, 30]. Whereas, when rutile has been used as a precursor, it has been observed to react incompletely [10, 11, 31], with not inconsiderable quantities of unreacted rutile remaining in the product after similar treatment conditions.

Crystalline TiO_2 has most commonly been used as a precursor in the production of nanotubes through alkaline hydrothermal treatment as amorphous TiO_2 precursors tend to produce amorphous materials rather than scrolled nanotubes [30, 32]. Crystallite size has previously been observed to influence the formation of the nanotubes, where smaller crystallite precursors convert into nanotubes at lower hydrothermal temperatures, concentrations, and treatment durations [9, 11]. This phenomenon is governed by the Kelvin effect, where smaller particles have greater solubilities than larger particles and are thus dissolved faster [33]. Precursor conversion and formation of nanotubes can also be influenced by the hydrothermal temperature [10], where elevating temperature increases the rate of precursor dissolution [33]. Thus, precursor dissolution has a significant impact on nanotube formation. Understanding of the influence of dissolution on nanotube formation will greatly impact the viability of scaled-up nanotube productions from readily available titania sources, such as natural rutile sands.

In this work, we determined the influence of the reactant chemistry in solution phase synthesis of titanate crystalline nanomaterials using commercial, crystalline-forms of anatase, and rutile titania as a starting material, with three main goals: (i) to determine the dissolution kinetics of the TiO_2 precursors, (ii) to determine the effect of surface area on the dissolution kinetics of TiO_2, and (iii) to determine the effect of TiO_2 precursor crystallite dissolution on the formation of titanate nanotubes.

Experimental procedure

Synthesis of nanotubes

Nanotubes were synthesized by alkaline hydrothermal treatment of commercial anatase and rutile precursors (Aldrich, ≥99.9% metals basis). The TiO_2 powders

(~0.5 g) were treated with aqueous sodium hydroxide (30 mL, 9 mol L^{-1}, 78% filling fraction). Once suspended, these solutions were sealed in PTFE-lined Parr autoclaves and statically heated in a convectional oven at 160 °C for 2, 4, 8, 16, and 32 h. The resultant product was then washed with aqueous hydrochloric acid (0.1 mol L^{-1}) and ultra-pure water (conductivity: 18.2 MΩ cm^{-1}) before drying by vacuum filtration.

Characterization of nanostructures

Pressed-powder XRD patterns were collected from all samples to determine sample composition. All samples were prepared using low background quartz depression mounts and analyzed using a PANalytical X'Pert PRO X-ray diffractometer operating at 40 kV and 40 mA using Cu radiation ($\lambda = 1.54060$ Å). The samples were analyzed using Bragg–Brentano geometry whilst spinning over a range of 5–70° 2θ with a step size of 0.0170° 2θ and a scan rate of 2.89° 2θ min^{-1}. Corundum (CR1, High Purity Alumina, Baikowski International Corporation) was used as either an internal or external standard to calibrate the absolute concentrations of the sample [34, 35]. When used as an internal standard, there was a 10:1 mixture of sample and corundum. A NIST1976 plate was used to track machine performance and to calibrate for variations of the instruments flux in cases where the external standard was not run at the same time as the sample. Rietveld analysis was performed using SiroQuant V3.0 (Sietronics Pty Ltd) [36] to determine the percent compositions of all materials. Crystallite sizes of the commercial anatase and rutile precursors were estimated through applying the Scherrer equation to the [101] and [110] reflections of anatase and rutile, respectively. A Perkin Elmer System 200 IR FT-Raman was used to acquire the Raman spectra using a Perkin Elmer diode pumped Nd:YAG laser. Samples were prepared as pressed pellets (4 mm diameter, 5 mm deep) and analyzed over 3800–200 cm^{-1}. The samples were imaged using a JEOL JEM-2010F TEM operated at 200 kV using a field emission gun electron source. The samples for TEM were prepared on holey carbon support films by placing a drop of sample resuspended in ethanol. Surface area analysis was performed on all samples through N_2 adsorption/desorption and calculated using the Brunauer–Emmet–Teller (BET) method. These analyses were measured on a Micromeritics TriStar 3000 Automated Gas Adsorption Analyzer after sample pre-treatment of heating at 110 °C overnight under N_2 atmosphere in order to remove adsorbed water from the surface. The particle size distributions of all samples were measured by dynamic light scattering using non-invasive back scattering technology using a Malvern Instruments Zetasizer Nano ZS. Sample preparation involved redispersing the powders within the hydrothermal mother liquor in the PTFE liner with a micro-Ti horn sonicator for 10 min directly after rapid cooling of the reaction vessel. The sample was then diluted and filtered through 0.45 and 0.1 μm filters (Millex HA, MF-Millipore MCE and Anotop 25, Whatman, respectively) into 3 mL disposable cuvettes for analysis.

Results and discussion

The reaction of TiO_2 precursors with NaOH and resultant nanotube formation was examined for a series of hydrothermal treatment times that ranged between 2 and 32 h. All sample products and their precursors were analyzed by XRD and FT-Raman spectroscopy to determine phase and composition. These techniques have been used previously to differentiate the phase (and associated morphology) of nanostructures formed after hydrothermal treatment [11]. Since the nanotube product and precursor nanoparticles both produce unique patterns in XRD and Raman spectra they can be easily differentiated from each other. The hydrothermal treatment of commercial anatase and rutile examined in this study was selected so as to exclusively yield a nanotube product.

To understand the effects of dissolution of the precursor on nanotube formation, a solid understanding of the precursor itself must be established. TiO_2 is known to exist as, or can be synthesized into eight polymorphic forms: anatase, rutile, brookite, TiO_2-B, TiO_2-R, TiO_2-H, TiO_2-II, and TiO_2-III [37]. Of the naturally occurring polymorphs, rutile is regarded as the most thermodynamically stable polymorph under ambient conditions [38], whereas anatase, brookite, and TiO_2-B are considered as metastable polymorphs which transform into rutile at elevated temperatures. However, solution-phase synthesis usually yields the anatase titania form. Under these conditions, nanoparticulate anatase has a lower surface energy than rutile and therefore thermodynamically has the lowest total energy compared to other TiO_2 polymorphs if the size domain is sufficiently small [1]. At the molecular level, the crystallographic configuration of anatase and rutile varies considerably. Although both unit cells are tetragonal, anatase consists of four TiO_2 units whereas rutile consists of two TiO_2 units. These TiO_2 units are comprised of a titanium atom coordinated to six neighboring oxygen atoms in an octahedral configuration, through two axial bonds and four equatorial bonds (anatase: 1.979 and 1.932 Å; and rutile: 1.976 and 1.946 Å, respectively) [39]. These TiO_6 octahedra are predominantly edge-sharing in anatase and corner-sharing in rutile. Due to the atomic configuration, the bonds in anatase suffer distortion compared to rutile. The densities of anatase and rutile also differ (3.9 and 4.17 g/mL) [40] and the average surface

energy of anatase is ca. 1.2 kcal mol^{-1} less stable than rutile [41].

Since previous studies have indicated that both the phase and the crystallite size influence the nanostructures formed through hydrothermal treatment [9, 10, 31], the commercially sourced precursors were analyzed by XRD to determine the phase composition and crystallite sizes. This analysis indicated that both precursors were phase-impure, containing minor phases of anatase (A), rutile (R), or amorphous material (am), and were determined to have the following crystallite size and percent compositions: anatase precursor (A) 112 ± 1 nm, 95%, (R) 140 ± 20 nm, 3%, (am) 2%; and rutile precursor (R) 320 ± 10 nm, 93%, (A) 220 ± 10 nm, 5%, (am) 2%.

After hydrothermal treatment, broad peaks of low intensity attributed to the titanate-like phase of nanotubes were observed in the XRD patterns in Fig. 1. These peaks ca. 9.7 and 24.5° 2θ were initially observed after 4 h for both the anatase- and rutile-treated powders (Fig. 1a(c), b(c) respectively). As the treatment duration was extended, the major nanotube-phase peaks ca. 9.7, 24.5, 28.3, and 48.2° 2θ were observed to increase in intensity and this coincided with a relative reduction of intensities from precursor reflections (correlated to ICDD # 01-71-1167 and 01-73-1232 for anatase and rutile, respectively). Complete reaction of each precursor was confirmed when the precursor reflections were not detected in the XRD patterns. Anatase was observed to completely react after 16 h of hydrothermal treatment for both commercial precursors, whereas rutile remained partly unreacted in the commercial rutile-treated powder after 32 h, even though it had completely reacted after 16 h in the anatase-treated powder. This variation in the reaction of rutile may be attributed to a number of factors, including the difference in the crystallite size and concentration of rutile in the two precursors.

FT-Raman investigations complemented the XRD analysis of the treated powders. Both anatase and rutile produce strong Raman spectra with moderate to strong intensity bands observed at 639, 516, 397, 144 cm^{-1} and 610, 449, 273, 235 cm^{-1}, respectively. Due to the Raman spectrometer's notch-filter cut-off, the strong intensity anatase E_g band at 144 cm^{-1} was not observable. Titanate nanotubes produce a unique spectrum with moderate to strong intensity bands at 699, 668, 445, 381, 285 and 271 cm^{-1}. In Fig. 2, the nanotube phase was observed after 4 h hydrothermal treatment of the anatase precursor through the presence of a peak at 445 cm^{-1} and a characteristic doublet occurring between 320 and 220 cm^{-1} [11]. When the treatment duration was increased these bands increased in intensity relative to the anatase bands at 639, 516, and 397 cm^{-1}, until 16 h treatment time when the anatase bands were no longer present. The results confirm the complete reaction of anatase precursor by 16 h

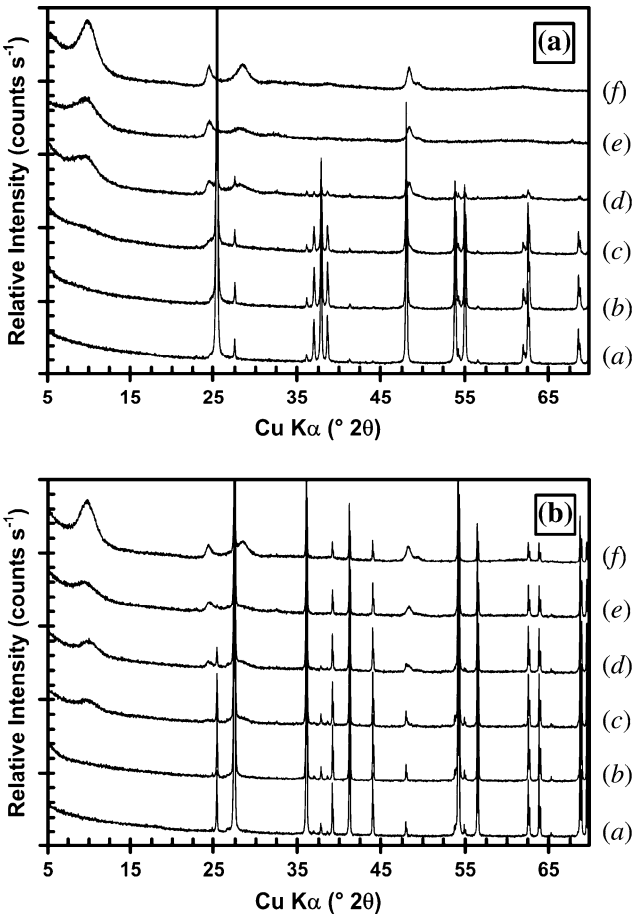

Fig. 1 XRD patterns of materials formed after 0 h (*a*); 2 h (*b*); 4 h (*c*); 8 h (*d*); 16 h (*e*); and 32 h (*f*) hydrothermal treatment of commercial anatase (**a**) and commercial rutile (**b**)

as was also indicated by the XRD analysis. Unlike anatase, the rutile signature bands in the rutile-treated powders overwhelmed the emerging nanotube bands due to the much greater Raman scattering capacity of rutile [11], the significant overlap of their band positions and also because a high concentration of unreacted rutile remained within the products after hydrothermal treatment. Therefore, the inability to determine the emission intensities of each phase in the rutile-treated powders prevented determination of nanotube concentration by Raman spectroscopy for the products of this precursor.

The formation of nanotubes was confirmed, however, through TEM investigations, where nanotubes were observed in all samples (2–32 h treatment duration). After short treatment times, titanate nanotubes were generally observed in the presence of significant quantities of nanoparticles and nanosheet-intermediate morphologies. In Fig. 3a, nanosheets and nanotubes appeared to adhere to and surround agglomerates of the residual precursor particles. These nanostructures did not appear to form through epitaxial growth from the nanoparticles; rather adhesion

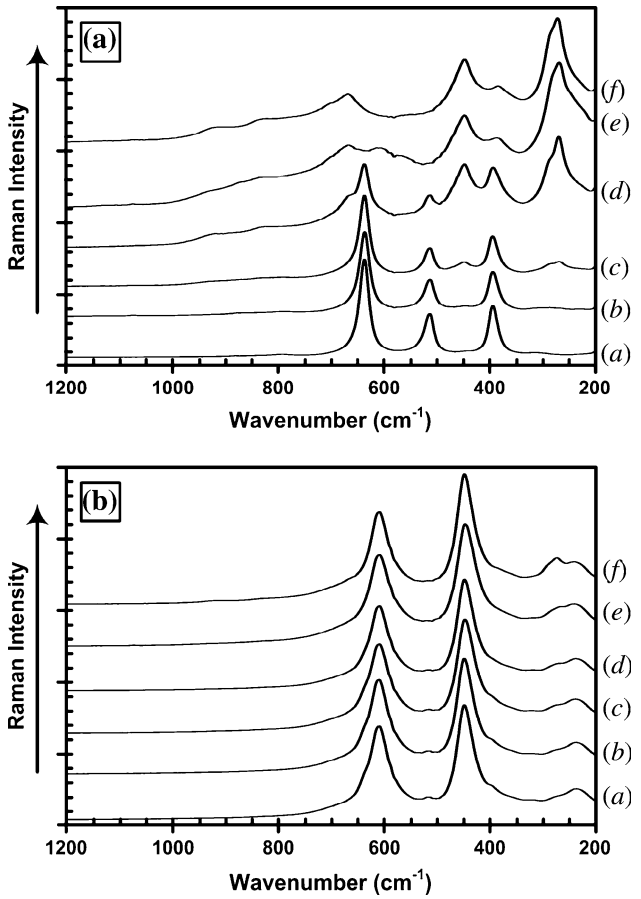

Fig. 2 Raman spectra of materials formed after 0 h (*a*); 2 h (*b*); 4 h (*c*); 8 h (*d*); 16 h (*e*); and 32 h (*f*) hydrothermal treatment of commercial anatase (**a**) and commercial rutile (**b**)

appeared to be caused through surface attractions between the already formed nanostructures. When treatment duration was increased, the ratio of nanotubes to nanoparticles also increased. Figure 3b depicts an agglomerate of well formed nanotubes produced from the anatase precursor at 8 h treatment duration. Anatase-produced nanotubes with an average internal diameter of 3.7 ± 0.7 nm, external diameter of 9.4 ± 1.7 nm, and lengths of up to several hundred nanometers. A high resolution image of an anatase-produced nanotube is portrayed in Fig. 3c. The walls of the nanotube are asymmetric, consisting of 6–7 shells (or layers) created through the axial scrolling of a single-layer titanate nanosheet. The rough, uneven surface of the nanotube indicates that the nanotube itself was also susceptible to the effect of dissolution by NaOH. Nanoparticles were also present in the 8 h anatase-treated powder, however, no nanoparticles were observed after 16 h hydrothermal treatment, confirmed by the absence of anatase in the XRD pattern. As the treatment duration was increased, there were no discernable changes within the nanotubes produced.

Although X-ray diffraction indicated that no nanotube reflections were present in the rutile-treated powder after 2 h, small quantities of nanotubes and nanosheets were observed by TEM investigation. After 4 h hydrothermal treatment, considerable quantities of well-formed nanotubes were observed for the rutile-treated powder as can be seen in Fig. 3d, e. Similar to the anatase-treated samples, these nanotubes appeared to cluster around nanoparticle aggregates. Rutile-produced nanotubes had an average internal diameter of 3.6 ± 0.7 nm, external diameter of 9.8 ± 1.5 nm, and lengths of up to several hundred nanometers. A high resolution image of a rutile-produced nanotube is presented in Fig. 3f, whose asymmetric walls consisted of 4–5 shells. All rutile-treated powders contained considerable quantities of nanoparticles as indicated by the presence of unreacted rutile in the XRD analysis.

When the specific surface areas of the products were analyzed, an increase in specific surface area was always observed in products corresponding to greater nanotube yields (as determined by XRD and Raman spectroscopy) for both the anatase- and the rutile-treated powders. Figure 4 presents the specific surface areas analyzed with nitrogen sorption using the Brunauer–Emmet–Teller (BET) calculations. The specific surface areas of the anatase-treated powders increased rapidly until a maximum of ca. 250 $m^2\ g^{-1}$ was reached for 8 h treatment before leveling out to ca. 220 $m^2\ g^{-1}$ between 16 and 32 h. The maximum in surface area measured for the 8 h treated powder suggests that nanosheets and partially formed nanotubes were present within the sample. Both of these nanostructures have greater specific surface areas than the fully formed nanotubes and can contribute up to a possible 25% increase in surface area compared to a sample containing fully formed nanotubes. This scenario is the probable cause of the increase in specific surface area as this sample contained ca. 6% unreacted anatase, which has a comparatively small surface area compared to the nanotubes. The presence of small quantities of nanosheets was observed within the 8 h treated anatase sample during the TEM investigation. An increase in specific surface area was also observed for the rutile-treated powders between 2 and 16 h of treatment after which no substantial increases were observed. These surface areas were significantly smaller compared to the anatase-treated powders. The origin of this lower surface area probably originated from the high concentrations of low surface area rutile particles remaining unreacted within the powder.

In accordance with the currently accepted mechanism of nanotube formation, the intermediate nanosheet morphology is believed to be constructed through the condensation and polymerization of mono- and polytitanic ions (TiO_3^{2-}, $TiO_2(OH)_2^{2-}$, and $Ti_nO_{2n+m}^{2m-}$) [42]. Through the reassembly of these titanic ions, it can be presumed that smaller,

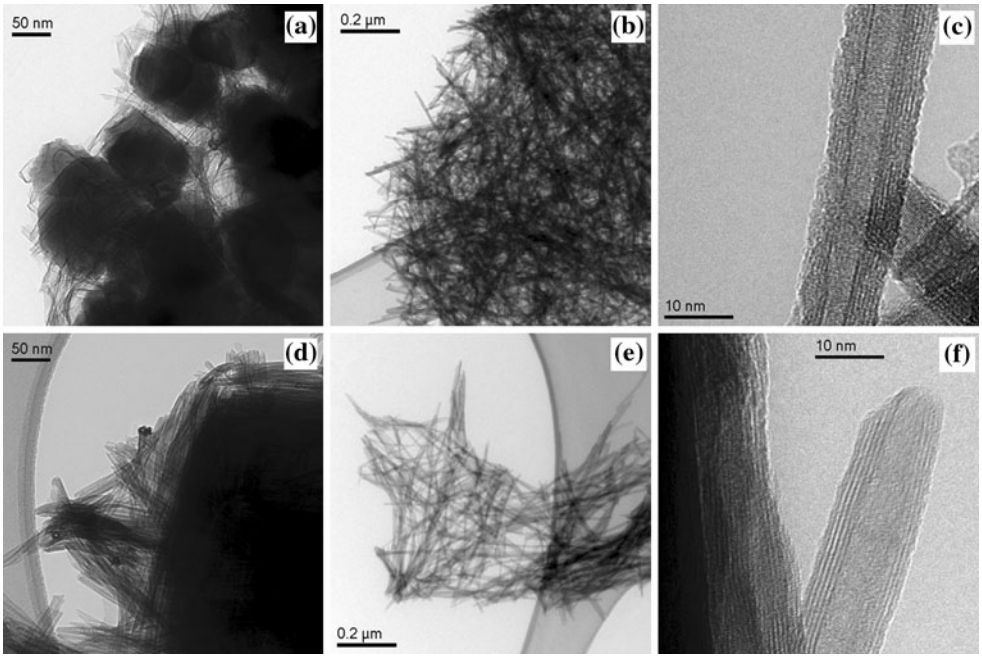

Fig. 3 TEM images of nanotubes formed from commercial anatase after 2 h (**a**) and 8 h (**b**, **c**) of hydrothermal treatment and from commercial rutile after 4 h (**d**–**f**) of hydrothermal treatment

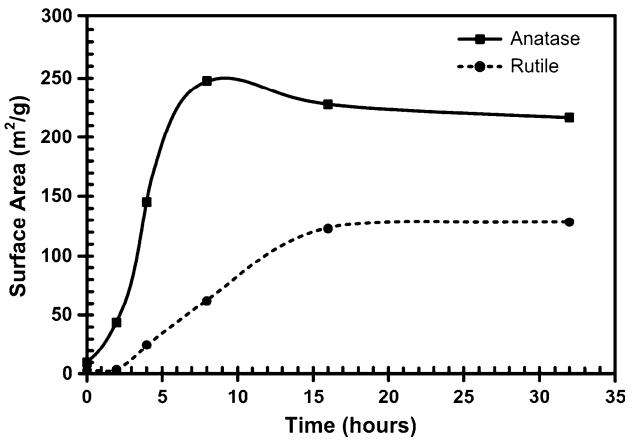

Fig. 4 BET surface areas of materials produced after hydrothermal treatment of commercial anatase and commercial rutile

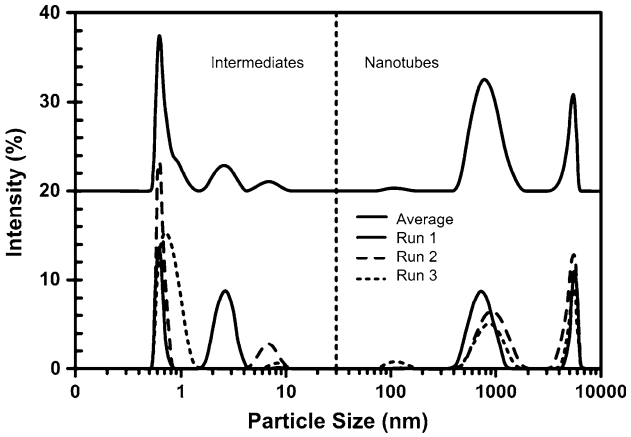

Fig. 5 Particle sizes of nanostructures formed after 2 h hydrothermal treatment of commercial rutile after filtering through 0.45 and 0.1 μm filters. Original traces of the three runs and their average are presented

intermediate nanosheet precursors may be produced within the hydrothermal liquor. To confirm this hypothesis, dynamic light scattering using non-invasive back scattering technology was performed on each hydrothermally treated sample to determine the particle size distributions of the nanostructures and their intermediates formed during hydrothermal treatment. To minimize the concentration of large particles and aggregates that could interfere with the detection of smaller particles, the samples were filtered through 0.45 and 0.1 μm Teflon filters. This process removed unreacted precursor particles >100 nm in diameter and large nanosheets whose dimensions exceeded 100 nm in height and width. In Fig. 5, multiple particle size distributions can be observed ranging between 0.6 and 6500 nm. Since the filtering process removed particles with a hydrodynamic radius of 100 nm or greater, these large particle size distributions could be produced by elongated structures with a width or diameter significantly less than 100 nm. We note that with diameters between 5 and 15 nm, some nanotubes could theoretically pass longitudinally through the filter pores, however their lengths can reach several hundred nanometers and it is more likely that the largest particle size distributions were generated by titanate nanotubes, possibly titanate nanotube aggregates. Over the duration of the analysis, the smaller particle size

distributions were observed to increase in intensity and thus decrease in concentration whilst the large particle size distributions increased in concentration. This suggests that these intermediates were actively reassembling into larger intermediates and nanotubes. These observations are consistent with the currently accepted mechanism of nanotube formation through the dissolution of the TiO_2 precursor and subsequent recrystallisation and scrolling of titanate sheets into nanotubes [18, 19, 42, 43].

Assuming the nanotubes form following the dissolution and subsequent recrystallisation of the particulate precursor [18], the decrease in the observed crystalline concentration over time could be attributed to precursor dissolution. The precursor dissolution products are Ti^{4+} species mainly in the form of mono- or polytitanic ions [42], where the concentration of dissolved Ti^{4+} species in solution is a function of temperature [19]. Nanosheets and nanotube formation occurs spontaneously [19, 44] when Ti^{4+} species are liberated from the precursor crystallites, and dynamic equilibrium is rapidly established between the Ti^{4+} species and the nanosheet intermediate [44]. As the nanosheet's surface charge is imbalanced because of undercoordinated sites [20], the nanosheets scroll or fold into nanotubes to neutralize this charge. Since nanotube formation is favored by this mechanism the reaction is constantly driven towards product formation. It can therefore be assumed that precursor dissolution is the rate determining step in the formation of nanotubes.

Rietveld analysis of the XRD peaks was performed on each sample to quantify the extent of precursor consumption and nanotube production after hydrothermal treatment. This was achieved through evaluating the residual crystalline content. As the exact phase of the nanotube titanate is not currently known, modeling of the nanotube XRD reflections for Rietveld analysis could not be performed, and the absolute amorphous and nanotube concentrations could not be determined. However, the TEM measurements did confirm that nanotube formation occurred in quantities commensurate with the quantities of precursor consumed. With these considerations, all Rietveld analyses for crystalline (precursor) and unmodeled phases (nanotube and amorphous content) are presented as wt% of the total sample (m/m %).

The kinetic order of precursor consumption was calculated for each precursor using the mass fraction of crystallite determined by Rietveld analysis over time (h). As suggested by interpretation of the intensity of the XRD patterns, anatase reacted quickly as evidenced by the rapid decrease of crystalline material with increasing treatment duration from 0 to 8 h in Fig. 6a. The observed rate of dissolution corresponds to zero-order kinetics (Linear regression of mass fraction versus time, $R^2 = 0.986$, see Fig. 6c) suggesting that the reaction was independent of the reactant concentration. In contrast to this result, a slow, non-linear decrease in crystalline concentration was observed for the rutile precursor with a ca. 67% decrease in crystalline content over 32 h treatment duration (Fig. 6b). This corresponds to a second-order dissolution rate (Linear regression of mass fraction^{-1} versus time, $R^2 = 0.999$, see Fig. 6d). These different kinetic orders of dissolution of anatase and rutile precursor materials are of primary interest because they highlight significant differences manifest in the mechanism of precursor consumption.

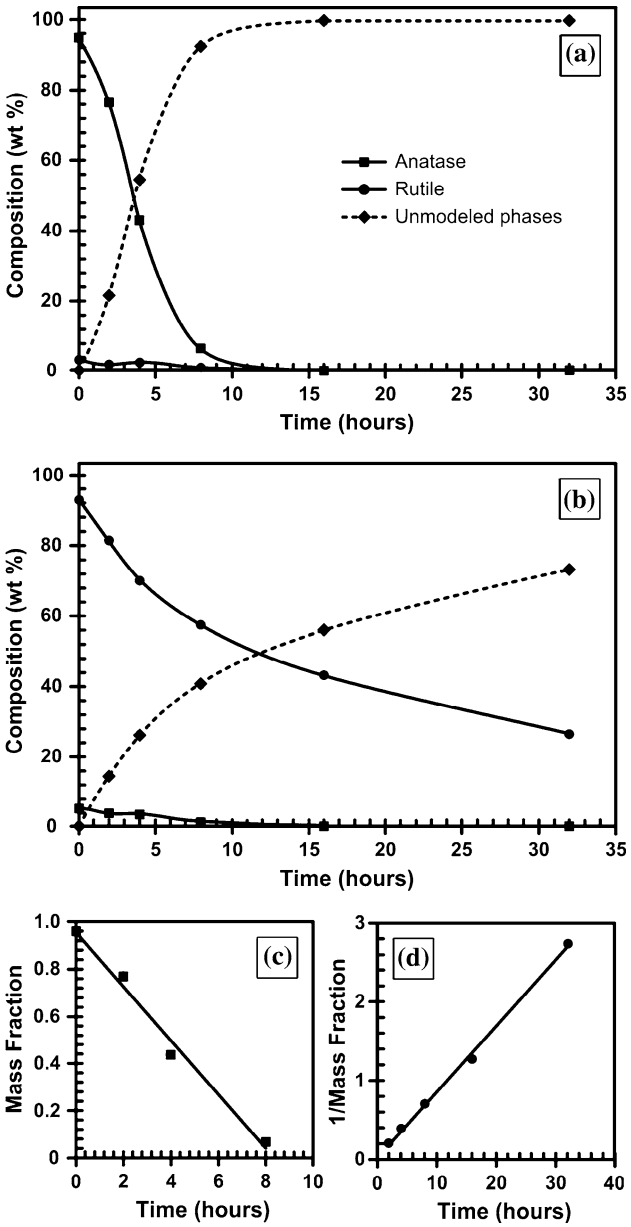

Fig. 6 Percent compositions of anatase, rutile and unmodelled phases (nanotubes and amorphous) content after hydrothermal treatment of commercial anatase (**a**) and commercial rutile (**b**); and their respective zero- (**c**) and second-order fittings (**d**)

To further examine the dissolution process, the effect of specific surface area over time was also examined. The specific surface areas of the unreacted precursors were calculated through Eq. 1, which is based on the specific surface area of a sphere [45], divided by the residual mass of the precursor, m (determined by Rietveld analysis).

$$\mathrm{SSA} = \frac{3}{\rho r m} \tag{1}$$

where ρ equals density ($m^2\ g^{-1}$), r equals radius (μm, calculated by applying the Scherrer equation to the [101] and [110] reflections of anatase and rutile, respectively), and m equals the mass of unreacted precursor (g). In these calculations, it is assumed that the particles are spherical in shape. Although these calculated values overestimated the specific surface area compared to the experimental results, the theoretical calculations are considered viable for the comparative estimation of surface area changes through the dissolution process. The relationship between specific surface area and time was determined to be first-order for both anatase and rutile precursors (see Fig. 7). Since the relationship of specific surface area to the observed dissolution kinetic orders varied (first-order compared to zero- and second-order), the shrinking spheres approximations could not be applied. The shrinking spheres approximation assumes that the rate of reaction is dependent only on the surface area of the dissolving solid [46]. This indicates that the increase in the dissolving precursor's specific surface area did not mediate the dissolution process. Although the anatase and rutile precursors have different surface areas and crystallite sizes ($9.89 \pm 0.03\ m^2\ g^{-1}$, 112 ± 1 nm and $2.33 \pm 0.02\ m^2\ g^{-1}$, 320 ± 10 nm, respectively), these parameters do not affect the overall kinetic order of dissolution, rather, they determine the rate constant of the reaction.

As the TiO_2 crystallites were completely immersed in concentrated NaOH, it is reasonable to assume that the TiO_2 surfaces become wetted to form a hydroxylated surface through the dissociative chemisorption of water. The OH^- ions in solution would then compete with the surface hydroxyl groups as ligands towards the metal ions at crystallite surface sites to weaken the critical metal–oxygen bonds [47]. Cleavage of the metal–ion centers would then occur once the surface site was sufficiently disturbed. The speciation of these hydroxylated Ti^{4+} metal ion complexes would be dependent on the degree of hydroxylation within the hexa-coordinate environment (e.g. $Ti(OH)_x^{4-x}$). Through this process, cleavage of mono- and polytitanic ions is also feasible (e.g. $TiO_2(OH)_2^{2-}$ and $Ti_nO_{2n+m}^{2m-}$). The Na^+ ion in solution could also influence the dissolution of the metal oxide through ion-exchange with the proton of the surface hydroxyls. This could result in the formation of partially substituted hydroxylated Ti^{4+} ion complexes. Reassembly of these ions and free Na^+ ions through condensation and polymerization processes would most likely produce a sodium titanate material, as proposed previously [18, 19]. Since the dissolved Ti^{4+} complexes and reassembles into a solid product (nanosheet), the hydrothermal liquor would never supersaturate with dissolved Ti^{4+}. This suggests that the dissolution of TiO_2 proceeds unhindered as nanotube product formation was observed to be favored under the conditions examined in this study.

The observed dissolution kinetics for the anatase precursor was determined to be zero-order whilst the dissolution process of rutile was second-order when treated with 9 mol L^{-1} NaOH at 160 °C. Zero-order kinetics indicates the dissolution process of anatase was independent of precursor concentration, and that dissolution was not restricted by the solubility of anatase [48]. The conversion of rutile has a linear relationship to time when applied to the parabolic diffusion model [49]. This suggests that the dissolution of rutile is affected by the diffusion of products away from, and the replenishment of reactant to the surface.

The variation of surface energies and atomic configurations could influence the dissolution kinetics of anatase and rutile. Anatase crystals are dominated by exposed (101) surfaces which can constitute greater than 94% of the crystal surface [41], whereas the predominantly exposed surface of rutile crystals are (110) planes, which can comprise between 50 and 80% of the crystals surface [41, 50]. Although the energies of these surfaces vary, the surface energies of rutile are generally greater than those of anatase [51]. This suggests that a greater driving force is required to liberate Ti^{4+} species from the rutile surface.

As both anatase and rutile are composed of TiO_6 octahedra it is conceivable that the mechanism of detachment of the hydroxylated metal center species during dissolution from the metal oxide surface would be identical. This implies that formation of nanotube structures occurs through the reassembly of similar intermediate building blocks, whether originating from anatase or rutile. Thus, it is plausible that nanotube formation occurs through the

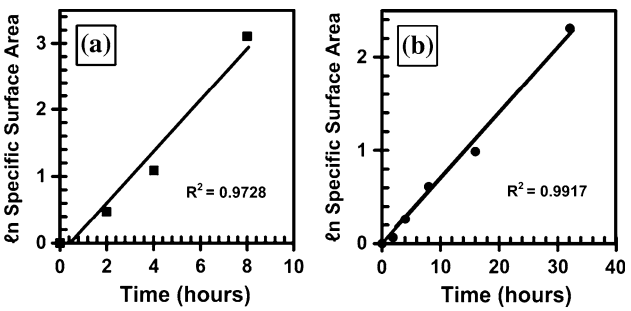

Fig. 7 First-order relationship of specific surface area to time for anatase (**a**) and rutile (**b**)

same kinetic process irrespective of the starting material. Considering that nanotubes and nanosheets have been observed to form after short treatment durations [52] and from low dissolved Ti^{4+} concentrations [53], this suggests that nanotubes form readily once Ti^{4+} species are liberated into solution. In this study, nanotubes were observed after all treatment durations for both anatase and rutile precursors. After 2 h hydrothermal treatment ca. 20 and 13% of the total crystalline component had dissolved for the anatase and rutile precursors, respectively. In both samples, commensurate quantities of nanotubes and nanosheets were observed in the TEM investigation. These results agree with the supposition that nanotubes form readily once liberated Ti^{4+} species are available in solution. This then implies that the observed latency in nanotube formation from rutile precursors is caused by the reduced availability of dissolved Ti^{4+} species in solution due to the slower second-order dissolution kinetics compared to the rapid zero-order dissolution of anatase. This variation in dissolution kinetics significantly influences nanotube syntheses from both natural and synthesized titania precursors as the slower second-order dissolution of rutile requires longer processing times than anatase to achieve 100% conversion of precursor to nanotubes. This has considerable ramifications towards the commercial viability of high-yield, large-scale processing of titanate nanostructures.

Conclusions

The dissolution kinetics of anatase and rutile and their effects on nanotube formation have been determined by examining products formed following hydrothermal reaction in 9 mol L^{-1} NaOH at 160 °C for a series of treatment durations. Anatase crystallites were observed to be consumed through zero-order kinetics, whereas the rutile precursor was consumed through a second-order process. The dissolution kinetics strongly influenced the formation of nanotubes which formed rapidly, in high yields from the fast, zero-order dissolution process of anatase, whilst reduced conversion was observed for the slower, second-order process of rutile. This dependence of the precursor dissolution on nanotube formation was related to the liberation of Ti^{4+} species into the solution. It was determined through a shrinking spheres approximation that the specific surface area of the precursor did not mediate the kinetic order of dissolution, indicating that the dissolution process was directly related to the phase of the precursor.

Acknowledgements The authors gratefully acknowledge financial support from the Australian Institute of Nuclear Science and Engineering through the provisioning of an award (AINGRA07051P) for access to research equipment at the Australian Nuclear Science and Technology Organisation. The financial and infrastructure support of the Queensland University of Technology, Discipline of Chemistry, is gratefully acknowledged. The Australian Research Council (ARC) is thanked for funding the instrumentation. Drs L. Rintoul and D. Cassidy are thanked for their assistance and expertise with the instrumentation used in this study. Dr R. A. Caruso is thanked for her understanding and support.

References

1. Reyes-Coronado D, Rodríguez-Gattorno G, Espinosa-Pesqueira ME, Cab C, de Coss R, Oskam G (2008) Nanotechnology 19:145605
2. Fujishima A, Zhang X, Tryk DA (2008) Surf Sci Rep 63:515
3. Maldotti A, Molinari A, Amadelli R (2002) Chem Rev 102:3811
4. Maira AJ, Yeung KL, Lee CY, Yue PL, Chan CK (2000) J Catal 192:185
5. Triani G, Evans PJ, Attard DJ, Prince KE, Bartlett JR, Tan S, Burford RP (2006) J Mater Chem 16:1355
6. Kasuga T, Hiramatsu M, Hoson A, Sekino T, Niihara K (1998) Langmuir 14:3160
7. Kasuga T, Hiramatsu M, Hoson A, Sekino T, Niihara K (1999) Adv Mater 11:1307
8. Elsanousi A, Elssfah EM, Zhang J, Lin J, Song HS, Tang C (2007) J Phys Chem C 111:14353
9. Morgado E Jr, De Abreu MAS, Moure GT, Marinkovic BA, Jardim PM, Araujo AS (2007) Chem Mater 19:665
10. Lan Y, Gao X, Zhu H, Zheng Z, Yan T, Wu F, Ringer SP, Song D (2005) Adv Funct Mater 15:1310
11. Morgan DL, Liu H-W, Frost RL, Waclawik ER (2010) J Phys Chem C 114:101
12. Niu HY, Wang JM, Shi YL, Cai YQ, Wei FS (2009) Microporous Mesoporous Mater 122:28
13. Prasad GK, Mahato TH, Singh B, Ganesan K, Srivastava AR, Kaushik MP, Vijayaraghavan R (2008) AIChE J 54:2957
14. Nian J-N, Chen S-A, Tsai C-C, Teng H (2006) J Phys Chem B 110:25817
15. Xu J-C, Lu M, Guo X-Y, Li H-L (2005) J Mol Catal A 226:123
16. Kavan L, Kalbáč M, Zukalová M, Exnar I, Lorenzen V, Nesper R, Grätzel M (2004) Chem Mater 16:477
17. Li J, Tang Z, Zhang Z (2006) Chem Phys Lett 418:506
18. Wang W, Varghese OK, Paulose M, Grimes CA (2004) J Mater Res 19:417
19. Bavykin DV, Parmon VN, Lapkin AA, Walsh FC (2004) J Mater Chem 14:3370
20. Saponjic ZV, Dimitrijevic NM, Tiede DM, Goshe AJ, Zuo X, Chen LX, Barnard AS, Zapol P, Curtiss L, Rajh T (2005) Adv Mater 17:965
21. Stumm W, Furrer G (1987) In: Stumm W (ed) Aquatic surface chemistry: chemical processes at the particle-water interface. Wiley, New York
22. Zhang Y, Walker D, Lesher CE (1989) Contrib Mineral Petrol 102:492
23. Lasaga AC, Luttge A (2001) Science 291:2400
24. Knauss KG, Dibley MJ, Bourcier WL, Shaw HF (2001) Appl Geochem 16:1115
25. Finnegan MP, Zhang HZ, Banfield JF (2008) Chem Mater 20:3443
26. Oskam G, Nellore A, Penn RL, Searson PC (2003) J Phys Chem B 107:1734
27. Chen Y-F, Lee C-Y, Yeng M-Y, Chiu H-T (2003) Mater Chem Phys 81:39
28. Seo D-S, Lee J-K, Kim H (2001) J Cryst Growth 229:428
29. Meng X-D, Wang D-Z, Liu J-H, Zhang S-Y (2004) Mater Res Bull 39:2163

30. Yuan Z-Y, Su B-L (2004) Colloids Surf A 241:173
31. Nakahira A, Kato W, Tamai M, Isshiki T, Nishio K, Aritani H (2004) J Mater Sci 39:4239. doi:10.1023/B:JMSC.0000033405.73881.7c
32. Kolen'ko YV, Kovnir KA, Gavrilov AI, Garshev AV, Frantti J, Lebedev OI, Churagulov BR, Van Tendeloo G, Yoshimura M (2006) J Phys Chem B 110:4030
33. Schmidt J, Vogelsberger W (2006) J Phys Chem B 110:3955
34. Hill RJ, Howard CJ (1987) J Appl Crystallogr 20:467
35. O'Connor BH, Raven MD (1988) Powder Diffr 3:2
36. Taylor JC (1991) Powder Diffr 6:2
37. Deng Q, Wei M, Ding X, Jiang L, Ye B, Wei K (2008) Chem Commun 3657
38. Swamy V, Gale JD, Dubrovinsky LS (2001) J Phys Chem Solids 62:887
39. Burdett JK, Hughbanks T, Miller GJ, Richardson JW Jr, Smith JV (1987) J Am Chem Soc 109:3639
40. CRC handbook of chemistry and physics (2009) vol 89th. CRC Press Inc., New York
41. Lazzeri M, Vittadini A, Selloni A (2001) Phys Rev B 63:155409/1
42. Wu D, Liu J, Zhao X, Li A, Chen Y, Ming N (2006) Chem Mater 18:547
43. Bavykin DV, Friedrich JM, Walsh FC (2006) Adv Mater 18:2807
44. Bavykin DV, Cressey BA, Light ME, Walsh FC (2008) Nanotechnology 19:275604/1
45. Lowell S, Shields JE, Thomas MA, Thommes M (2004) Characterization of porous solids and powders: Surface area, pore size and density. Kluwer Academic, Dordrecht
46. Marabi A, Mayor G, Burbidge A, Wallach R, Saguy IS (2008) Chem Eng J 139:118
47. Schindler PW, Stumm W (1987) In: Stumm W (ed) Aquatic surface chemistry: chemical processes at the particle-water interface. Wiley, New York
48. Chida T, Niibori Y, Tochiyama O, Mimura H, Tanaka K (2004) Mater Res Soc Symp Proc 824:467
49. Tikhov SF, Sadykov VA, Ratko AI, Kouznetsova TF, Romanenkov VE, Eremenko SI (2007) React Kinet Catal Lett 92:83
50. Mendive CB, Bredow T, Feldhoff A, Blesa MA, Bahnemann D (2008) Phys Chem Chem Phys 10:1960
51. Zhang HZ, Banfield JF (1998) J Mater Chem 8:2073
52. Yang J, Jin Z, Wang X, Li W, Zhang J, Zhang S, Guo X, Zhang Z (2003) Dalton Trans 3898
53. Bavykin DV, Walsh FC (2007) J Phys Chem C 111:14644